CELL BIOLOGY

Concurrent processes set *E. coli* cell division

Gabriele Micali[1,2]*, Jacopo Grilli[3]*, Matteo Osella[4,5], Marco Cosentino Lagomarsino[6,7,8]†

A cell can divide only upon completion of chromosome segregation; otherwise, its daughters would lose genetic material. However, we do not know whether the partitioning of chromosomes is the key event for the decision to divide. We show how key trends in single-cell data reject the classic idea of replication-segregation as the rate-limiting process for cell division. Instead, the data agree with a model where two concurrent processes (setting replication initiation and interdivision time) set cell division on competing time scales. During each cell cycle, division is set by the slowest process (an "AND" gate). The concept of transitions between cell cycle stages as decisional processes integrating multiple inputs instead of cascading from orchestrated steps can affect the way we think of the cell cycle in general.

INTRODUCTION

Correct chromosome replication and segregation are necessary for cell division to ensure that genetic material is propagated correctly (*1*, *2*). In bacteria such as *Escherichia coli*, a known pathway prevents cells from dividing if the chromosomes interfere with the cytokinesis machinery (*3*). However, whether completion of segregation is typically the bottleneck process for the decision to divide has never been stringently tested on single cells (*4*).

New dynamic single-cell data have revived the classic debate on the determinants of cell division, but the recent literature is fragmented into different and contrasting models (*4*). Most studies take the classic view (*5*) that after a size-regulated "B period" from cell division to initiation of replication, a fixed "C + D period," comprising a "C period" to copy the genome and a "D period," needed to complete segregation and running from termination to cell division (Fig. 1A), is rate limiting for cell division (Fig. 1B), but these studies do not agree on the underlying mechanisms (*6*, *7*). A recent study by Harris and Theriot (*8*) formulates the opposite hypothesis. The main assumption of this alternative view is that the rate-limiting process for cell division is instead the completion of the septum (Fig. 1B); consequently, chromosome segregation is never rate limiting for cell division.

More specifically, the authors provide evidence that surface synthesis rate is proportional to volume; they propose a model where division is set by a threshold surface to synthesize the septum (*8*). This model recapitulates the empirical size control strategy followed by these cells, whereby the added size is nearly constant, regardless of initial size (the so-called adder behavior) (*8*–*10*). With these contrasting results, the question of which process drives cell division becomes pressing (Fig. 1B). Our central finding is that both processes occur concurrently to set cell division (Fig. 1, C and D).

RESULTS

To support this point, we started our analysis from the available experimental data. Single-cell growth in these data is well described by an exponential, with some cell-to-cell variability in the growth rate (*9*, *11*). We have focused on two underrated correlation patterns measured recently for the C + D period. Figure 2 (A and B) shows these patterns. First, we find that the growth of the cell during the C + D period, quantified by the log ratio of the division volume and the initiation volume, is anticorrelated with cell size at initiation (Fig. 2A). This pattern is very consistent across strains, measurement methods, and conditions, but is overlooked by current models, which assume that replication is the bottleneck process (*6*, *7*). Second, we find that the duration of the C + D period is anticorrelated with the growth rate of individual cells, with a near-inverse relationship (Fig. 2B), as reported by Wallden and coworkers (*6*). We note that, because of experimental limitations, the termination event has not always been recorded and, in most cases, only the cumulative C + D period is available. However, available experimental data (*12*) indicate that coupling of growth in the C + D period with initiation size mainly comes from the D period.

These patterns are not compatible with the classic assumption of replication driving division: There are no available justifications for these correlations between timing and either growth rate or cell size. If replication is always the bottleneck process, then division should occur on average at a fixed time after initiation of replication. Assuming that this fixed time is not coupled to cell size or growth rate, both plots in Fig. 2 (A and B) would show no correlation (Fig. 2, C and D, orange lines). Note that the plot in Fig. 2A is equivalent to testing the correlation of the final volume with initiation volume or of the added volume during C + D with initiation volume (*13*, *14*). For example, if replication is always the bottleneck process and division happens at a fixed average time after initiation of replication, then we expect the final volume to be maximally correlated to initiation volume, but this is not the case in the data.

In contrast, the C + D patterns emerge naturally from a model in which the division event is set by two concurrent processes. In a concurrent processes framework, the C + D period is the juxtaposition of two processes: the time by which the replication-related process is ready to divide, defined as C + D′, and the time by which the cell interdivision process (e.g., the septum) is completed. The measurable C + D is the time for the cell to really divide and is set at the single-cell level by the slowest between these two processes. Whenever division is set by the cell-related interdivision process, the cells that initiate replication at a larger size will grow less during the C + D period (because, in this case, the final size ignores the initiation size), which gives the pattern of Fig. 2A. Equally, each time the interdivision process is slowest, the D period will tend to be shorter for cells growing faster than average due to the size-based interdivision control. For example, if the interdivision process adds an average constant size (*8*, *9*), this target size will be reached faster by single cells growing faster than average, which will decrease the duration of their C + D period. This yields the pattern shown in Fig. 2B.

[1]Department of Environmental Microbiology, Eawag, Dübendorf, Switzerland. [2]Department of Environmental Systems Science, ETH Zürich, Zürich, Switzerland. [3]Santa Fe Institute, 1399 Hyde Park Road, Santa Fe, NM 87501, USA. [4]Physics Department, University of Turin, Via Giuria 16, Torino, Italy. [5]I.N.F.N., Torino, Italy. [6]Sorbonne Universités, UPMC University Paris 06, Paris, France. [7]CNRS, UMR 7238, Paris, France. [8]IFOM, FIRC Institute of Molecular Oncology, Milan, Italy.
*These authors contributed equally to this work.
†Corresponding author. Email: marco.cosentino-lagomarsino@ifom.eu

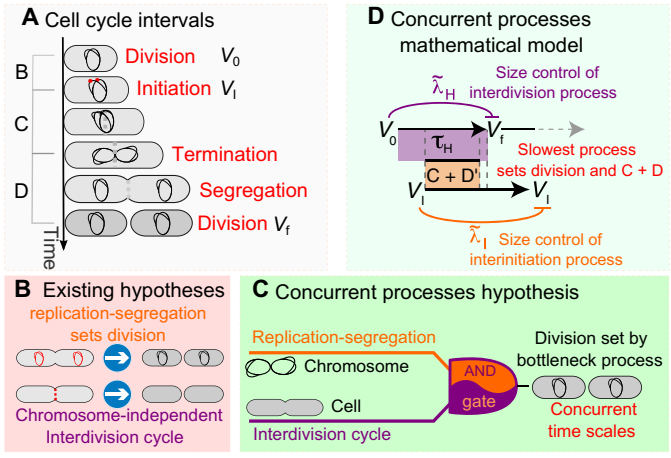

Fig. 1. The concurrent processes hypothesis. (**A**) Explanation of the replication-related cell cycle intervals in *E. coli*. Replication initiation occurs after a B period, followed by the C (replication) and D (termination to division) periods, and the B and C + D periods can be measured in single cells by proxies of replication initiation (*6*, *12*). (**B**) Classically, replication-segregation is believed to be rate limiting for cell division; a recent hypothesis by Harris and Theriot (*8*) states that the rate-limiting process might be instead the formation of the septum. (**C**) Our concurrent processes hypothesis states that cell division is the result of the slowest between a cell-related interdivision process (setting division when, e.g., the septum machinery is ready) and a chromosome-related process (setting division when replication-segregation is complete). Hence, the circuit is analogous to an AND gate. (**D**) Scheme of the mathematical model.

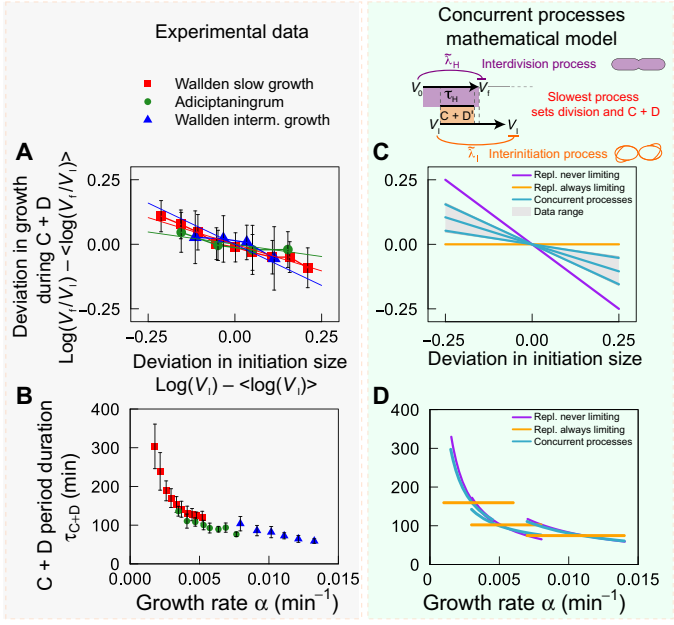

Fig. 2. A concurrent processes model explains the correlation patterns for the C + D period. (**A**) and (**B**) plot the unexplained patterns for the C + D period. (A) Cell growth during the C + D period, quantified by the logarithmic ratio between the final and initial volume (*y* axis, binned averages), anticorrelates with cell size at initiation (*x* axis). The plot is centered by the mean values of the *x*- and *y*-axis variables to compare different datasets. Solid lines are linear fits. (B) The duration of the C + D period (*y* axis, binned averages) anticorrelates with the growth rate of individual cells (*x* axis), with a near-inverse pattern. (**C**) The correlation between size at initiation and growth during the C + D period (A) attains the observed intermediate slopes (gray shaded area) in the concurrent processes hypothesis (cyan lines; see Materials and methods for parameters), but not if one assumes that replication is always (orange line) or never limiting (purple line) cell division. Solid lines correspond to theoretical predictions, and the shaded area to the range of slopes allowed by the plots in (A). (**D**) The anti-correlation between C + D period duration and growth rate of individual cells (B) is absent if replication is always bottleneck (orange line). Instead, the concurrent processes hypothesis captures experimental trends quantitatively [cyan lines have the same parameters as in (B); see Materials and methods]. Solid lines correspond to theoretical predictions. Data are from (*6*, *12*).

To go beyond these qualitative considerations, and to produce testable quantitative predictions on the assumption of concurrent processes setting cell division, we formulated and solved a mathematical model based on this principle (see Materials and methods). In this model, two size-dependent processes exist. A chromosome process setting initiation and a cell-related process trying to set division run in parallel, and division follows the slowest process (as in an AND gate) between completion of the interdivision process and completion of a C + D′ period after initiation (Fig. 1D). We note that the available data do not allow us to make a clear distinction between the different chromosome-related processes (e.g., DNA replication and segregation). Biologically, cell division is limited by nucleoid occlusion (*3*, *15*); hence, a chromosome-aware cell division process should be limited at least by completion of segregation. Our minimal description of the chromosome cycle complies with the classic view and posits that a size-uncoupled C + D period is minimally required to divide after initiation. However, things could be more complex (*16*). Future, more detailed, data on cell cycle transitions in single cells may help to develop more mechanistic models of the decisional process leading to cell division.

We solve the model both analytically and by numerical simulation. Figure 2 (C and D) shows the predicted patterns of the C + D period (light blue lines). The model reproduces both correlation patterns shown in Fig. 2 (A and B). Figure 2C also shows that when replication is limiting, both slopes are flat (Fig. 2, C and D, orange lines), indicating that the classic framework is too restrictive. Instead, models, assuming that replication is never limiting (*8*), may reproduce the trends in Fig. 2 (A and C), but the slope is quantitatively too strong for the data in Fig. 2A. Specifically, if replication is never limiting, then the size at division V_f is independent from the size at initiation V_I. The growth between initiation and division (*y* axis of Fig. 2A) is $\log(V_f/V_I) = \log(V_f) - \log(V_I)$. If $\log(V_f)$ is independent of V_I (because replication is never limiting), then the slope is equal to −1. The data reside in the intermediate regime, where competition between the two processes setting cell division is relevant. While one cannot rule out all possible scenarios, it is possible to show that available models, assuming that replication-segregation is always limiting for cell division, fail to reproduce these patterns [see (*17*), which provides an extensive technical analysis comparing different models]. Wallden and coworkers (*6*) take the growth rate dependence of the C + D period in Fig. 2B as a basic assumption. However, their model still fails to reproduce Fig. 2A. Overall, the concurrent processes assumption explains the patterns for the C + D period naturally from the conceptually simple assumption of competing time scales between the different processes that set cell division.

The fact that the model captures the data does not depend on a specific parameter set but emerges from the hypothesis of concurrent processes. This point can be shown by direct analytical estimates of the patterns in Fig. 2 (see Materials and methods for details). Our model (see Fig. 1D and Materials and methods) is specified by the two size control parameters $\tilde{\lambda}_I$ and $\tilde{\lambda}_H$ [ranging from 0 (strong control) to 1 (no control)], by the characteristic initiation and division sizes

encoded by the two concurrent processes, and by the intrinsic cell-to-cell stochasticity of their duration (see Materials and methods). The values of these parameters affect the probability p_H that the interdivision process is rate limiting, which is the only relevant emergent parameter of the model. For any parameter set, the plots in Fig. 2 depend on p_H only: They deviate from constancy if replication is not always limiting, i.e., when p_H deviates from 0, and the case of replication never limiting ($p_H = 1$) appears quantitatively too extreme to fit the data. In the data, we estimate from the slopes that p_H is between 0.25 and 0.75 (see Materials and methods), well within the parameter region in which there is actual competition between the two processes. Thus, regardless of parameter values and details, only competing time scales efficiently reproduce the data.

We found that similar conclusions apply to other testable predictions of the model, beyond the C + D period. First, the model predicts that competition between concurrent processes should affect the relation between the growth in the B and C + D periods. To test this prediction, we use the method introduced by Chandler-Brown and coworkers in yeast (*18*), comparing growth (measured here by log ratio of final to initial volume) in the two periods. If replication is never limiting, then fluctuations in the initiation size make the B period longer and the C + D period shorter, affecting, in opposite directions, growth in the B and C + D periods, which become anticorrelated. If replication is always limiting, then growth in the C + D period should instead be independent from growth in the B period. Our results show that the concurrent processes model predicts an intermediate situation between these two, which is where all the data are found (Fig. 3, A and B). The argument to understand the slopes in Fig. 3B is similar to the one that explains the slope of Fig. 2A. The growth during C + D, $\log(V_f/V_I)$ (plotted on the *y* axis), can be expressed as the difference of the growth during the whole cycle and the growth during the B period, $\log(V_f/V_I) = \log(V_f/V_0) - \log(V_I/V_0)$. If replication is never limiting, then $\log(V_f/V_0)$ is independent of $\log(V_f/V_I)$, while $\log(V_I/V_0)$ and $\log(V_f/V_I)$ are in a linear relation with slope one. Equivalently, if the size at initiation is irrelevant for the size at division, then the growth in the B period must be anticorrelated (with slope −1) to the growth in the C + D period. If instead replication is always limiting, then the growth during the C + D period is uncoupled to both size at initiation and initial size, hence independent on $\log(V_I/V_0)$. Second, competition between concurrent processes should also affect measurable patterns for the interdivision cycle, where abundant data are available. Motivated from the trend in Fig. 2B, we focused on the anticorrelation reported between interdivision time and individual cell growth rates (*19*). Our results (Fig. 3, C and D) show that the model captures the decreasing trend of this correlation with average growth rate. Once again, rather than the specific numerical values of the parameters, we find that the data take intermediate values between the two extreme cases of replication always or never limiting division.

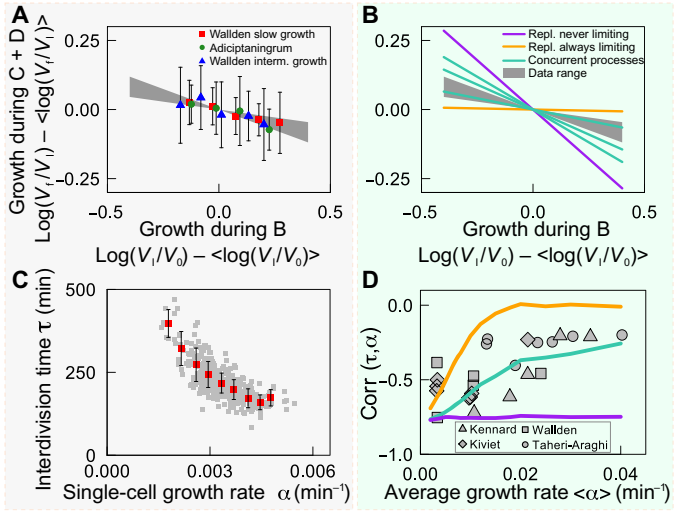

Fig. 3. Predictions of the concurrent processes model beyond the C + D period are verified in data. (**A**) In the data, growth quantified by logarithmic final to initial size ratio in the C + D period has a weak negative correlation with growth in the B period [see (*18*)]. (**B**) This correlation falls in the range where the replication and interdivision processes compete to set cell division (cyan lines; obtained with the same parameters as in Fig. 2, B and D, listed in Materials and methods). (**C** and **D**) The negative correlation of interdivision time with individual cell growth rate [exemplified for one dataset in (C)] has a decreasing trend with increasing growth rate, captured by the model (cyan line; $p_H = 0.25$; other parameters were fixed as in the other figures; see Materials and methods). Cell cycle subperiod data are from (*6*, *12*). Interdivision cycle data [in (D)] are from (*6*, *10*, *19*, *28*).

DISCUSSION

In *E. coli*, the average cell size varies across conditions, but the average size per replication origin at initiation remains nearly constant (*20*). This old observation was recently proven to be very robust to perturbations (*21*, *22*). Classically, this observation was interpreted as evidence for a replication-limited cell division circuit (*5*, *20*). However, since we have shown that single-cell behavior challenges this interpretation, the classic view needs to be revisited. In the hypothesis of concurrent processes, different processes (e.g., a chromosome cycle and an interdivision cycle) are sometimes the slowest to be completed and set cell division in a given condition. This also translates into a concurrence of size scales and can happen if the characteristic division sizes encoded by the different processes are similar. However, since mean cell size per origin is roughly constant across conditions, we can surmise that the division size encoded by the chromosome process has to grow with population growth rate, along with the number of origins. If this hypothesis applies, then the size scale of the cell-related interdivision process also has to grow, or concurrence would be lost by varying the growth media. In addition, different analyses indicate that a single size scale governs the whole size distribution across conditions [a behavior called "scaling" (*10*, *13*, *19*)], suggesting either a matching or a perfect dominance of a single encoded size.

If the two size scales encoded by a chromosome cycle and a cell-related interdivision cycle are coupled, causation could act in either (or both) directions, i.e., the characteristic cell size could be caused by the encoded initiation size per origin, or vice versa (or be the result of a mutual coupling) (*23*, *24*). Notably, deletion of the nucleoid occlusion SlmA, which prevents division in the presence of unsegregated chromosomes, leaves mean cell size unaffected (*3*, *15*), in line with the idea that the replication-associated process does not always drive cell division. The exact causal (and temporal) chain of events might be detectable by examining single cells under perturbations and during nutrient shift experiments. Last, if we abandon the long-standing assumption that replication initiation always drives cell division in *E. coli* favoring a scenario of concurrent processes, then we are forced to rethink the regulatory process linking replication to cell division (*23*), and alternative hypotheses should be revisited in data (*16*, *25*).

More generally, following the pioneering views of Boye and Nordström (*23*), our findings support a change of perspective on the cell

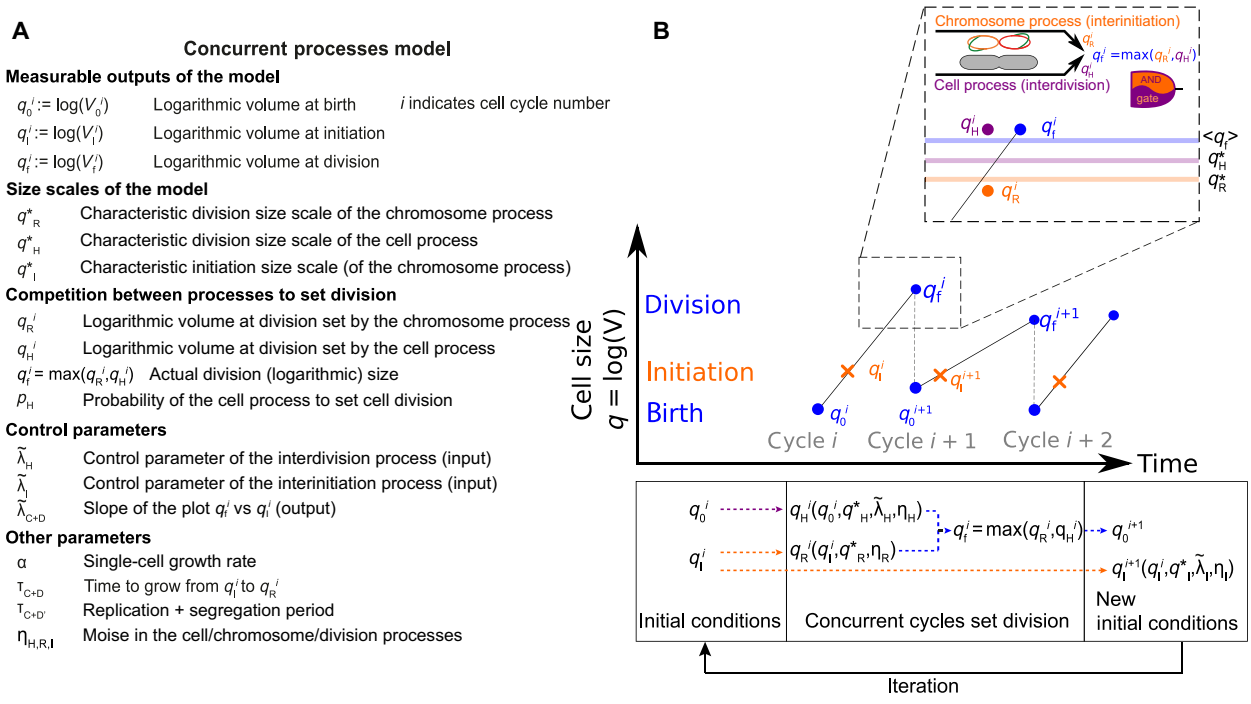

Fig. 4. Parameter definitions and illustration of the concurrent processes model. (**A**) Definition of size variables and control parameters used in the model. (**B**) Implementation of the concurrent process model. Schematic (top) and algorithm (bottom). In the cell process (purple), q_0^i sets a desired final size q_H^i, while in the chromosome process (orange), the initiation size q_I^i sets both the initiation size q_I^{i+1} and a desired final size q_R^i. To set the actual final size q_f^i (blue), the cell and chromosome process compete through q_H^i and q_R^i, and the largest desired size (or, equivalently, the slowest process) sets cell division. Once the division size of cycle i, and hence the size at birth of the cycle $i + 1$, is set, new size-coupled stochastic division and initiation events are programmed for the next cell cycle.

cycle. We can draw a comparison with the way the cell cycle is described in animal cells. A prevalent narrative of the cell cycle, particularly for (higher) eukaryotes, is a succession of well-determined transitions under a common master clock. However, this paradigm struggles to find the "final trigger" of cell cycle intervals (*26*). Instead, in line with our concurrent processes view, emerging evidence supports the idea that a key aspect could be the integration of multiple decisions (*26*, *27*). For example, cell division in higher eukaryotes requires coordination of the actin cortex and the spindle (*27*), with required cross-talk between these two systems that is analogous to the one addressed here. The concept of concurrent processes on competing time scales can be important to characterization of cell cycle stages other than division, as well as the cell cycles of other organisms. We expect that this different perspective will affect future analyses of the coordination of cell division and other cell cycle stages with metabolic and physiological cues.

MATERIALS AND METHODS

Data analysis

Figures 2 and 3 (A and C) use data on SeqA foci formation from (*6*, *12*). The data contain information on cell division, size versus time, and replication initiation time of single tracked cells. Figure 3D also uses datasets from (*6*, *10*, *19*, *28*). The data contain information on cell division and size versus time of single tracked cells for a total of about 10^6 cells. The dataset in (*6*) contains about 400 cells in the slow growth condition and about 90 pairs of mother-daughter cells in the intermediate growth condition. The dataset in (*12*) contains 80 cells. For the slow growth data in (*6*) and for (*12*), cells typically have a single DNA replication round during a cell division cycle, and mother-daughter tracking is not necessary. For the intermediate growth conditions of (*6*), cells typically have two overlapping rounds of DNA replication, and mother-daughter tracking is needed to define the C + D period, because it spans two cell cycles. The plots in Figs. 2 and 3 show binned averages (where the *x*-axis variable was subdivided into bins of equal size); the averages of the *y*-axis variables were considered only for bins containing more than five data points.

Mathematical model and analytical predictions

We describe here the mathematical framework for the concurrent processes model and the main analytical results (see Fig. 4). We point the reader with modeling expertise to related work, where a similar framework was established to study interdivision correlations (*13*, *14*), and to a related manuscript addressed to a technical audience, where the same formalism is used for a detailed comparison of the models available in the literature (*17*).

Control parameters and their interpretation

Figure 4A shows a list of the variables and control parameters of the model. To quantify the coupling between size and cell cycle progression (and growth) for each cell cycle interval X, the model uses the control parameters $\tilde{\lambda}_X$. These parameters range from 0 (size threshold) to 1 (timer, no size control). The value of $\tilde{\lambda}_X$ can be estimated as the slope of the plot of final versus initial logarithmic size during the cell cycle interval. For example, $\tilde{\lambda}_{C+D}$ is the slope of the plot of the logarithmic size at division versus the logarithmic size at initiation. Equivalently, $\tilde{\lambda}_{C+D}$ is one minus the slope of the so-called size-growth plot (*29*) of relative growth during a cell cycle interval versus the cell size at the entry of the interval (see Fig. 2, A and C).

In the model, initiation of replication is set by a size-coupled process acting between consecutive initiations, with a control parameter $\tilde{\lambda}_I$, which describes the strength of the size correction. When $\tilde{\lambda}_I = 1/2$, initiation follows an adder (*7*), while for $\tilde{\lambda}_I = 0$, initiation is triggered by a critical size (*6*) (a sizer).The case of overlapping rounds of DNA replication (*30*) is described by this model by the assumption that the initiation circuit encodes a size in units of replication origins (*7*). Similarly, division size is set by a process with control parameter $\tilde{\lambda}_H$, which is an adder when $\tilde{\lambda}_H = 1/2$.

The qualitative predictions of the model are very robust to variations in the actual mechanisms of cell cycle progression, e.g., whether initiation is controlled by a sizer per origin or an adder per origin, or something else, specified by the parameters $\tilde{\lambda}_I$ and $\tilde{\lambda}_H$ in the model. This point can be shown by direct analytical estimates.

Stochasticity

Stochasticity parameters describe size-independent cell-to-cell variability in duration of the interdivision and interinitiation processes. The "C + D′" period duration is assumed to be a size-independent Gaussian random variable with assigned mean and variance (a "timer"). Last, cells are assumed to grow exponentially, and the growth rate is a random variable with prescribed distribution (e.g., Gaussian).

Formulation of the model

The model (see Fig. 4B) is composed of two concurrent stochastic processes: An interdivision process sets a possible division (log) size q_H (or equivalently a division time) as a function of the size at birth, and a chromosome cycle defines the initiation size q_I, and thus also indirectly a concurrent possible division time (and size q_R) compatible with the termination of replication and segregation.

The defining equations of the model are

$$\begin{aligned} q_H^i &= q_H^* + \tilde{\lambda}_H \delta q_H^{i-1} + \alpha \eta_H^{i-1} \\ q_I^i &= q_I^* + \tilde{\lambda}_I \delta q_I^{i-1} + \alpha \eta_I^{i-1} \end{aligned} \tag{1}$$

where i is a cell cycle index (the cell with index i is a daughter of the cell with index $i-1$), $q_X = \log(V_X)$ are logarithmic sizes, and $\delta q_X = q_X - \langle q_X \rangle$ are fluctuations. The two parameters q_H^* and q_I^* set the characteristic division and initiation size scales of the two concurrent processes. Last, η_X are noises describing cell-to-cell variability (the growth rate α is a random variable in our simulations but, for simplicity, will be considered constant in the following calculations). Equation 1 states that size at division and size at initiation are corrected by the interdivision and interinitiation processes, respectively, with control parameters $\tilde{\lambda}_I$ and $\tilde{\lambda}_H$ (*13*).

The logarithm of the final size encoded by the replication-related process in a given cell cycle i, q_R, can be expressed as

$$q_R^i = q_I^i + \alpha \tau_{C+D'} \tag{2}$$

which can be rewritten as

$$q_R^i = q_R^* + \delta q_I^i + \alpha \eta_R^i \tag{3}$$

where

$$q_R^* = \langle q_R \rangle = \langle q_I \rangle + \alpha \tau_{C+D'} \tag{4}$$

and $\tau_{C+D'}$ is the time for the replication-related process to be ready for cell division.

The concurrent processes condition states that the final size is the one dictated by the slowest process; hence

$$q_f^i = \max\left(q_H^i, q_R^i\right) \tag{5}$$

Mean-field approximation

To compute the effective final size, we rewrite Eq. 5 as

$$q_f^i = q_H^i s^i + q_R^i (1 - s^i) \tag{6}$$

where s^i is a random variable with values in {0,1}. The probability that s^i is 1 depends on q_0 and q_I. We consider the approximation where $s^i = 1$ with probability p_H independently of q_0 and q_I (but dependently on their averages $\langle q_0 \rangle$ and $\langle q_I \rangle$ and noises, see below). We verified that this approximation (which we refer to as "mean-field" approximation) works very well with simulations in the noise range of empirical data. p_H is the probability that the interdivision process is rate limiting, a relevant outcome of the model (depending on the parameters), and is estimated below.

Predictions of the model

In this model, the value parameter $\tilde{\lambda}_{C+D}$ is not an input but the result of the interplay between the concurrent processes. It is measured by the slope of Fig. 2 (A and C) or equivalently by the covariance

$$\left\langle \delta q_f^i \, \delta q_I^i \right\rangle =: \tilde{\lambda}_{C+D} \sigma_{q_I}^2 \tag{7}$$

where $\sigma_{q_I}^2$ is the variance of the logarithmic initiation size. The equivalence between these two definitions is explained as follows. Figure 2 (A and C) implies the condition $\delta q_f^i = \tilde{\lambda}_{C+D} \delta q_I^i + \xi_{C+D}^i$ (where ξ_{C+D} is an effective noise term characterizing the cell-to-cell variability). Computing the covariance between the two fluctuations leads to Eq. 7.

Some algebra on the combination of Eqs. 1, 6, and 7, leads to the equation

$$\tilde{\lambda}_{C+D} = \frac{1 - p_H}{1 - p_H \tilde{\lambda}_H \tilde{\lambda}_I} \tag{8}$$

The ratio in the right-hand side of Eq. 8 is strictly 1 when $p_H = 0$ (i.e., replication is always rate limiting) and strictly 0 when $p_H = 1$ (i.e., replication is never limiting). Instead, intermediate values of this ratio can only be attained for intermediate values of p_H for many combinations of the other parameters. Note that Eq. 8, given $\tilde{\lambda}_H$ and $\tilde{\lambda}_I$, allows us to directly estimate p_H. In the data, since empirically $\tilde{\lambda}_H \approx 1/2$, we estimate that $p_H \approx 0.24$ to 0.69 for a sizer at initiation ($\tilde{\lambda}_I \approx 0$) and $p_H \approx 0.3$ to 0.75 for an adder between initiations ($\tilde{\lambda}_I \approx 1/2$).

Let us now consider the pattern in Fig. 2B. When replication sets division (with probability $1 - p_H$), the mean initiation volume $\langle V_I \rangle$ dictates the duration of the C + D period (which corresponds to the C + D′ period) independently on the growth rate; when replication is not the bottleneck (with probability p_H), the final size will be initiation independent and encoded by the interdivision process $\langle V_H \rangle$, and for a fixed growth rate α, the duration of the C + D period will be proportional to $(1/\alpha)(\langle q_H \rangle - \langle q_I \rangle) =: \chi/\alpha$, where χ is roughly the log ratio of the sizes encoded by the two processes $\chi \approx \log(\langle V_H \rangle / \langle V_I \rangle)$ [assuming that

$\log(\langle V_X \rangle) \approx \langle q_X \rangle$, which is valid for small noise (*7*, *13*)]. The effective duration of the C + D periods is estimated as

$$\langle \tau_{C+D} | \alpha \rangle \simeq (1 - p_H)\langle \tau_{C+D'} \rangle + p_H \frac{\chi}{\alpha} \quad (9)$$

Equation 9 is approximate because, at the fixed single-cell growth rate, the probability that the interdivision sets division varies compared to p_H (which is its average value).

Equation 9 predicts that the duration of the period is a sum between a constant and an inverse relationship with the single-cell growth rate. The assumption that replication limits division can only predict the constant part, at odds with the data. Conversely, Fig. 2 shows how the data are in line with the predictions of the concurrent processes model.

Equation 9 contains $\langle q_H \rangle$ and $\langle \tau_{C+D'} \rangle$, neither of which is directly accessible from experiments. We could turn it in an expression containing the final (log) size $\langle q_f \rangle$, which is measured directly in experiments. Equation 6, under the mean-field approximation described above, gives

$$\langle q_f \rangle = p_H \langle q_H \rangle + (1 - p_H)(\langle q_I \rangle + \langle \alpha \rangle \langle \tau_{C+D'} \rangle) \quad (10)$$

where we have used independence of C + D′ duration. Substituting this expression in Eq. 9, yields

$$\langle \tau_{C+D} | \alpha \rangle \simeq (1 - p_H)\langle \tau_{C+D'} \rangle \left[1 - \frac{\langle \alpha \rangle}{\alpha} \right] + \frac{\langle q_f \rangle - \langle q_I \rangle}{\alpha} \quad (11)$$

which can be solved for the only unknown parameter, the product $(1 - p_H)\langle \tau_{C+D'} \rangle$ to estimate its value from the data, leaving no adjustable parameters for the predictions shown in Fig. 2D.

Model parameters

We discuss here the values of the model parameters used in the plots and how they were fixed. The cyan lines in Fig. 2C represent theoretical predictions and have a negative slope corresponding to Eq. 8 with p_H = 0.48, 0.3, and 0.75 for an adder between initiations (see below), respectively, for the Wallden *et al.* slow growth, Adiciptaningrum *et al.*, and Wallden *et al.* intermediate growth datasets (*6*, *12*). These values were fixed from Fig. 2A and Eq. 8. The same values of p_H are used in all other plots. In Fig. 2D, the orange lines are the best fit for the case where replication is limiting [corresponding to the model of (*7*)]. The average duration of the C + D period is set from the empirical averages to 160, 102, and 75 min for the Wallden *et al.* slow growth, Adiciptaningrum *et al.*, and Wallden *et al.* intermediate growth datasets, respectively. Cyan curves follow Eq. 9 with p_H fixed as above, and $\langle \tau_{C+D'} \rangle$ was fixed from Eq. 11 to the following values: 49 min (Wallden *et al.* slow growth), 52 min (Adiciptaningrum *et al.*), and 41 min (Wallden *et al.* intermediate growth).

Figure 3 (B and D) shows the result of numerical simulations, where the parameters were constrained from the data. The plots in Fig. 2 fix the values of p_H and $\langle \tau_{C+D'} \rangle$ for the three datasets in Fig. 3B, while Fig. 3D corresponds to a wide range of growth conditions and required more general choices. Specifically, the numerical simulations use the following input parameters, directly fixed from the data: (i and ii) The average growth rate $\langle \alpha \rangle$ and its variance σ^2_α. In Fig. 3D, the average growth rates range from 0.002 to 0.04 min^{-1} to match the experimental values. The variance of the growth rate was chosen by keeping a constant coefficient of variation (CV) of 0.15. The growth rate was a normal or log-normal random variable (the two choices do not affect the results, see below), extracted independently for every cell cycle. (iii and iv) The average added volume per origin between consecutive initiations $\langle v_I \rangle$ and its variance $\sigma^2_{v_I}$. The average added volume per origin was fixed to 0.45 μm^3 as measured in (*6*), and the variance was fixed to a constant CV of 0.15. The added volume between consecutive initiations was assumed to be log-normally distributed (and extracted independently for every cell cycle). (v and vi) The average time needed for replication and segregation (the C + D′ period) $\langle \tau_{C+D'} \rangle$ and its variance $\sigma^2_{\tau_{C+D'}}$. In Fig. 3D, the average duration of the C + D′ period was set to 45 min independently from the average growth rate, and its CV was maintained constant and equal to 0.2 for the simulations corresponding to replication always limiting (orange lines) and concurrent processes (cyan lines). The average duration of the C + D′ period was set to 0 for the simulations where replication is never limiting (purple lines). $\tau_{C+D'}$ was assumed to be a normal random variable (extracted independently for every cell cycle). Note that the average added volume per origin between consecutive initiations, the average growth rate, and the average C + D′ duration set the characteristic division size of the interinitiation process, $q^*_R \approx \langle \log(v_I) \rangle + \langle \tau_{C+D'} \rangle \langle \alpha \rangle$. (vii and viii) The average interdivision added volume $\langle \Delta_H \rangle$ and its variance $\sigma^2_{\Delta_H}$. Note that $\langle \Delta_H \rangle$ sets the characteristic size of the interdivision process q^*_H. In Fig. 3B, $\langle \Delta_H \rangle$ was fixed to achieve the same values of p_H as in Fig. 2 (B and D). In Fig. 3D, the interdivision added volume was fixed so that for the case of concurrent cycles, the replication-related process and the interdivision process would compete to set division in the same way across all conditions. Specifically, we chose $\langle \Delta_H \rangle = \langle v_I \rangle \exp(45 \text{ min} \cdot \langle \alpha \rangle)$ for the case of concurrent processes (Fig. 3D, cyan line). The case where replication is never limiting (purple line) was simulated by assuming the same $\langle \Delta_H \rangle$ but setting $\tau_{C+D'}$ to zero. Last, we set $\langle \Delta_H \rangle = 0$ to simulate the case of replication always limiting (orange line). With these choices, $p_H \approx 0$ for the replication always limiting case (Fig. 3D, orange line), $p_H \approx 0.6$ for concurrent cycles (cyan line), and $p_H \approx 1$ for the replication never limiting models (purple line). The variance $\sigma^2_{\Delta_H}$ was set to a constant CV of 0.15 over the different growth conditions. The interdivision volume was assumed to be a log-normally distributed random variable as above.

We chose to present the data with $\tilde{\lambda}_I = \tilde{\lambda}_H = 1/2$ (adder) simulations, but we explored other values of these parameters, and in particular $\tilde{\lambda}_I = 0$ and $\tilde{\lambda}_H = 1/2$, initiation triggered at fixed size per origin, finding very robust results. In addition, while Fig. 3 follows a specific set of parameters, we explored systematically in simulations different characteristic sizes and noise levels for the two processes. For instance, as mentioned above, the simulations for Gaussian-distributed growth rate, interdivision volume, and added volume per origin between consecutive initiations show no substantial differences in the trends shown in Fig. 3 (data not shown).

REFERENCES AND NOTES

1. M. Meselson, F. W. Stahl, The replication of DNA in *Escherichia coli*. *Proc. Natl. Acad. Sci. U.S.A.* **44**, 671–682 (1958).
2. P. Nurse, Y. Masui, L. Hartwell, Understanding the cell cycle. *Nat. Med.* **4**, 1103–1106 (1998).
3. T. G. Bernhardt, P. A. J. de Boer, Slma, a nucleoid-associated, ftsz binding protein required for blocking septal ring assembly over chromosomes in *E. coli*. *Mol. Cell* **18**, 555–564 (2005).
4. M. Osella, S. J. Tans, M. Cosentino Lagomarsino, Step by step, cell by cell: Quantification of the bacterial cell cycle. *Trends Microbiol.* **25**, 250–256 (2017).

5. W. D. Donachie, Relationship between cell size and time of Initiation of DNA replication. *Nature* **219**, 1077–1079 (1968).
6. M. Wallden, D. Fange, E. G. Lundius, Ö. Baltekin, J. Elf, The synchronization of replication and division cycles in individual *E. coli* cells. *Cell* **166**, 729–739 (2016).
7. P.-Y. Ho, A. Amir, Simultaneous regulation of cell size and chromosome replication in bacteria. *Front. Microbiol.* **6**, 662 (2015).
8. L. K. Harris, J. A. Theriot, Relative rates of surface and volume synthesis set bacterial cell size. *Cell* **165**, 1479–1492 (2016).
9. M. Campos, I. V. Surovtsev, S. Kato, A. Paintdakhi, B. Beltran, S. E. Ebmeier, C. Jacobs-Wagner, A constant size extension drives bacterial cell size homeostasis. *Cell* **159**, 1433–1446 (2014).
10. S. Taheri-Araghi, S. Bradde, J. T. Sauls, N. S. Hill, P. A. Levin, J. Paulsson, M. Vergassola, S. Jun, Cell-size control and homeostasis in bacteria. *Curr. Biol.* **25**, 385–391 (2015).
11. A. Adiciptaningrum, M. Osella, M. C. Moolman, M. Cosentino Lagomarsino, S. J. Tans, Stochasticity and homeostasis in the *E. coli* replication and division cycle. *Sci. Rep.* **5**, 18261 (2015).
12. M. Osella, E. Nugent, M. Cosentino Lagomarsino, Concerted control of *Escherichia coli* cell division. *Proc. Natl. Acad. Sci. U.S.A.* **111**, 3431–3435 (2014).
13. J. Grilli, M. Osella, A. S. Kennard, M. Cosentino Lagomarsino, Relevant parameters in models of cell division control. *Phys. Rev. E* **95**, 032411 (2017).
14. J. Grilli, C. Cadart, G. Micali, M. Osella, M. Cosentino Lagomarsino, The empirical fluctuation pattern of *E. coli* division control. *Front. Microbiol.* **9**, 1541 (2018).
15. H. Cho, H. R. McManus, S. L. Dove, T. G. Bernhardt, Nucleoid occlusion factor SlmA is a DNA-activated FtsZ polymerization antagonist. *Proc. Natl. Acad. Sci. U.S.A.* **108**, 3773–3778 (2011).
16. N. E. Kleckner, K. Chatzi, M. A. White, J. K. Fisher, M. Stouf, Coordination of growth, chromosome replication/segregation, and cell division in *E. coli*. *Front. Microbiol.* **9**, 1469 (2018).
17. G. Micali, J. Grilli, J. Marchi, M. Osella, M. C. Lagomarsino, Dissecting the control mechanisms for DNA replication and cell division in *E. coli*. *Cell Rep.* **25**, 761–771 (2018).
18. D. Chandler-Brown, K. M. Schmoller, Y. Winetraub, and J. M. Skotheim, The adder phenomenon emerges from independent control of pre- and post-*Start* phases of the budding yeast cell cycle. *Curr. Biol.* **27**, 2774–2783.e3 (2017).
19. A. S. Kennard, M. Osella, A. Javer, J. Grilli, P. Nghe, S. J. Tans, P. Cicuta, and M. Cosentino Lagomarsino, Individuality and universality in the growth-division laws of single *E. coli* cells. *Phys. Rev. E* **93**, 012408 (2016).
20. W. D. Donachie, G. W. Blakely, Coupling the initiation of chromosome replication to cell size in *Escherichia coli*. *Curr. Opin. Microbiol.* **6**, 146–150 (2003).
21. H. Zheng, P.-Y. Ho, M. Jiang, B. Tang, W. Liu, D. Li, X. Yu, N. E. Kleckner, A. Amir, C. Liu, Interrogating the *Escherichia coli* cell cycle by cell dimension perturbations. *Proc. Natl. Acad. Sci. U.S.A.* **113**, 15000–15005 (2016).
22. F. Si, D. Li, S. E. Cox, J. T. Sauls, O. Azizi, C. Sou, A. B. Schwartz, M. J. Erickstad, Y. Jun, X. Li, S. Jun, Invariance of initiation mass and predictability of cell size in *Escherichia coli*. *Curr. Biol.* **27**, 1278–1287 (2017).
23. E. Boye, K. Nordström, Coupling the cell cycle to cell growth: A look at the parameters that regulate cell-cycle events. *EMBO Rep.* **4**, 757–760 (2003).
24. S. Cooper, *Bacterial Growth and Division: Biochemistry and Regulation of Prokaryotic and Eukaryotic Division Cycles* (Academic Press, 1991).
25. D. Bates, N. Kleckner, Chromosome and replisome dynamics in *E. coli*: Loss of sister cohesion triggers global chromosome movement and mediates chromosome segregation. *Cell* **121**, 899–911 (2005).
26. N. Mchedlishvili, K. Jonak, A. T. Saurin, Meeting report—Getting into and out of mitosis. *J. Cell Sci.* **128**, 4035–4038 (2015).
27. N. Ramkumar, B. Baum, Coupling changes in cell shape to chromosome segregation. *Nat. Rev. Mol. Cell Biol.* **17**, 511–521 (2016).
28. D. J. Kiviet, P. Nghe, N. Walker, S. Boulineau, V. Sunderlikova, S. J. Tans, Stochasticity of metabolism and growth at the single-cell level. *Nature* **514**, 376–379 (2014).
29. S. Di Talia, J. M. Skotheim, J. M. Bean, E. D. Siggia, F. R. Cross, The effects of molecular noise and size control on variability in the budding yeast cell cycle. *Nature* **448**, 947–951 (2007).
30. S. Cooper, C. E. Helmstetter, Chromosome replication and the division cycle of *Escherichia coli* B/r. *J. Mol. Biol.* **31**, 519–540 (1968).

Acknowledgments: We are very grateful to N. Kleckner, C. Cadart, S. van Teeffelen, A. Amir, B. Sclavi, S. Tans, and I. Iuliani for their feedback. **Funding:** This work was supported by the International Human Frontier Science Program Organization (grant HFSP RGY0070/2014). M.O. was supported by the "Departments of Excellence 2018–2022" grant awarded by the Italian Ministry of Education, University and Research (MIUR) (L. 232/2016). J.G. was supported by an Omidyar Postdoctoral Fellowship at the Santa Fe Institute. G.M. was supported by grant nr. 31003A_169978 from the Swiss National Science Foundation to Martin Ackermann. **Author contributions:** M.C.L., M.O., G.M., and J.G. designed the research and contributed with key ideas and analyses at different stages. G.M. relentlessly performed data analysis, model simulations, and analytical calculations. J.G. provided a forceful drive for the analytical calculations. M.C.L. conceived the project and wrote the paper, with constant help and feedback from the other authors. **Competing interests:** The authors declare that they have no competing interests. **Data and materials availability:** The code used to simulate the concurrent cycles model is available on Mendeley Data and can be accessed at https://data.mendeley.com/datasets/tgvykrrph4/. All other data needed to evaluate the conclusions in the paper are present in the paper and/or the Supplementary Materials. Additional data related to this paper may be requested from the authors.

Submitted 30 May 2018
Accepted 3 October 2018
Published 7 November 2018
10.1126/sciadv.aau3324

Citation: G. Micali, J. Grilli, M. Osella, M. Cosentino Lagomarsino, Concurrent processes set *E. coli* cell division. *Sci. Adv.* **4**, eaau3324 (2018).

Concurrent processes set *E. coli* cell division

Gabriele Micali, Jacopo Grilli, Matteo Osella and Marco Cosentino Lagomarsino

Sci Adv **4** (11), eaau3324.
DOI: 10.1126/sciadv.aau3324